Handwriting Tracking using 60 GHz mmWave Radar

Sai Deepika Regani*†, Chenshu Wu*†, Feng Zhang*†, Beibei Wang*†, Min Wu*† and K.J. Ray Liu*†

*Department of Electrical and Computer Engineering,
University of Maryland, College Park, MD-20742.
†Origin Wireless Inc., 7500 Greenway Center Drive, Suite 1070, MD 20770, USA.
Email: rdeepika@terpmail.umd.edu, {chenshu.wu, feng.zhang, beibei.wang}@originwireless.net,{minwu, kjrliu}@umd.edu.

Abstract—Human-computer interaction is a vital component in today's world and there is a constant quest for automated and user-friendly techniques for interaction. Handwriting is one of the most general and natural ways of interaction for humans. While handwriting recognition is a well-studied problem, its counterpart handwriting tracking is still being investigated. Most of the existing handwriting tracking systems either require sensors attached to the hand or involve specially designed hardware. In this work, we propose a handwriting tracking system that reuses a commodity 60GHz Wi-Fi radio as a radar. The moving target is localized at each time instance and a trajectory is constructed by connecting those location estimates. While the digital beamforming technique and the pulsed radar are used to recover the spatial and range information, Doppler velocity is used to isolate the moving target from the static objects. Further, subsample peak interpolation and smoothing techniques enhance the overall performance of the proposed system. Extensive experiments demonstrate an average tracking error of 2.5% of the distance from the device and validate the robustness of the system to different environments and experimental conditions.

I. Introduction

A rapid increase in automation fueled the quest for more efficient and user-friendly approaches that aid Human-Computer Interaction (HCI). Smart surfaces and touch screens have emerged as a more user-friendly alternative to the traditional input devices such as the keyboard and the computer mouse. But in an era where we are surrounded by numerous smart connected devices, usually in small form factors, the space for human-computer interaction cannot be limited by dedicated hardware such as the touch screens. Instead, we are seeing an increasing trend of ubiquitous interactions with machines via in-the-air gestures, handwriting and voice-controllable systems, which is also evidenced by recent industrial efforts including Microsoft Kinect [1], Google Soli [2], Apple UWB radar, Apple Siri, Amazon Alexa, Google Home, etc. Handwriting is a generalized form of a gesture and a natural way of interaction for the humans and serves as an attractive approach for HCI. Provided the mature handwriting recognition [3], enabling pervasive and accurate tracking of handwriting in the air or on the board will realize innumerable applications in the field of HCI.

Handwriting tracking refers to recovering the trajectory traced by a target of interest and can be done either actively or passively. In active tracking systems, a sensor is mounted on the moving target and the trajectory is recovered from the sensor information. For instance, accelerometers in mobile phones have been used to recover trajectories drawn in the air [4]. RF-IDRAW uses RFID tags fixed on the user's hand to achieve multi-resolution positioning [5]. On the other hand, in passive tracking, the user is not required to wear or carry any electronic device. The sensor, be it a camera or a Wi-Fi radio, is fixed on a static reference and the trajectory traced by the moving target is recovered from the recorded sensor information. Due to user convenience, passive tracking systems are preferred over the active tracking systems. Most of the passive tracking systems are camera-based and usually aim to track a pen or finger-tip to determine the writing trajectory [6]. However, all the camera-based approaches lead to potential privacy concerns and may not work in low ambient light.

Radio waves cover a significant portion of the electromagnetic (EM) spectrum ranging from 30 Hz to 300 GHz and enable a wide range of applications. The one most relevant to this work is the Wi-Fi communication. The 802.11 standard provides different frequency bands at 2.4 GHz and 5 GHz for Wi-Fi, which were exploited in the past to achieve wireless sensing applications such as motion detection, vital sign monitoring, human identification, indoor localization, etc. [7], [8]. The performance, however, is fundamentally limited by the bandwidths, antenna number, and carrier frequencies. With the advent of the 5G technology and the accessibility to the mmWave band (30 GHz-300 GHz), achieving higher resolutions became possible. Since EM waves can easily surpass objects smaller than their wavelength, mmWaves offer this unique advantage of being able to reflect signals off a pen or a finger thereby tracking changes at the millimeter scale. Another advantage offered by the mmWaves is the fewer number of multipath due to their heavy attenuation and easy absorption by different surfaces. Also, such a high bandwidth (few GHz) allows high resolution in the temporal domain, which can distinguish between the arrival times of different multipath. Owing to the aforementioned advantages, we propose a handwriting tracking system using a commercial 60 GHz mmWave radar.

mTrack [9] is the most relevant existing work that can passively track handwriting using the 60 GHz radio waves. However, the system requires calibration and specially designed multiple transceivers. Also, *mTrack* requires special

surfaces to absorb reflected signals and minimize background reflections. To the best of our knowledge, this is the first work to use a single commercial 60 GHz mmWave radar to achieve fine-grained handwriting tracking. The main contributions of this work can be summarized as follows:

- We propose a handwriting tracking system using a single commercial 60 GHz radar. This is a privacy-preserving, precise, robust and calibration-free system that can enable a writing surface on top of any flat surface or in the air.
- We present a complete end-to-end system to retrieve handwritten characters within regions as small as 1 cm x 1 cm.
- We perform extensive experiments to analyze the performance of the proposed system in different experimental conditions and environments.

This paper is organized as follows. Section II presents the preliminary information required for this work. Section III describes the different stages of the handwriting tracking algorithm in detail. Section IV demonstrates the performance of the proposed system through various experiments and finally, Section V concludes the paper.

II. PRELIMINARIES
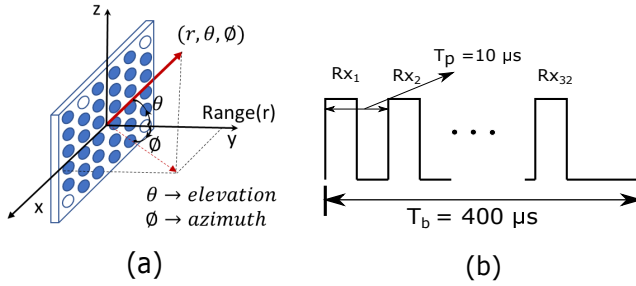
A. The 60 GHz radar

Fig. 1: (a) Coordinate system of the radar, (b) One burst consisting of 32 pulses.

In this work, we use Qualcomm's 60 GHz mmWave radar, which reuses a commercial 60GHz Wi-Fi chip by attaching an extra antenna array, to record the channel impulse response (CIR) time series during handwriting and process it to obtain the handwriting trajectory. It is a monostatic pulsed radar consisting of 32 transceivers. The 32 antennas are arranged in a 6×6 grid with a separation of 3 mm between the adjacent pair of antennas. The arrangement of the 32 transceivers and the coordinate system of the radar is shown in Fig. 1a. In this work, we use 1 transmitting antenna and 32 receiving antennas.

The pulsed radar emits electromagnetic waves in the form of short pulses which are reflected by different objects and captured by the receiver antenna. A group of 32 pulses is termed as a burst. The reflected pulse of each of the 32 pulses in a burst is received by a different receiving antenna as demonstrated in Fig. 1b. The figure shows one burst consisting of 32 pulses. The duration of each pulse is $T_\mathrm{p} = 10 \ \mu s$ and the
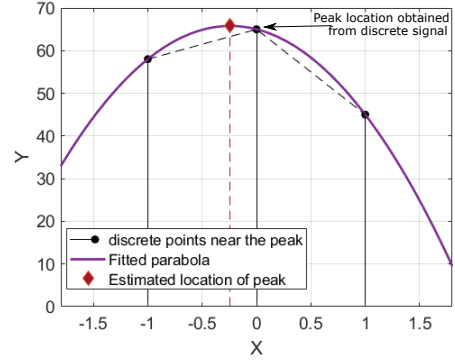

Fig. 2: Subsample peak interpolation.

duration of each burst is $T_\mathrm{b} = 400 \ \mu s$. The burst dimension is known as the slow-time dimension in the radar literature while the time dimension corresponding to the CIR taps is known as the fast-time. A bandwidth of BW = 3.52 GHz allows a time resolution of Δt = 0.28 ns and hence a range accuracy of $\frac{c\Delta t}{2} = 4.261$ cm, where c is the speed of light.

B. Subsample Peak Interpolation (SPI)

The location of the maximum value of a signal is of great significance in several applications and Subsample Peak Interpolation (SPI) is one of the common approaches to determine the location of the peak value at sub-sample accuracy. For example, SPI finds applications in time-of-flight estimation [10], power spectral peak estimation [11], delay estimation from correlation peaks [12] and etc. One of the widely used methods for SPI is the parabolic interpolation at the location of the peak. Fig. 2 shows an example of SPI. The circular points in black are the three data points of the discrete signal at the location of the peak. From the discrete signal values, the location of the peak is at $X = 0$. By performing parabolic interpolation near the peak using the peak value and the two samples adjacent to the peak, the new location of the peak is estimated. The point in red shows the new location of the peak which is the vertex of the fitted parabola. SPI plays a significant role in accurate estimation of the location of the target which will be demonstrated in Section III.

III. HANDWRITING TRACKING ALGORITHM

The aim of the proposed algorithm is to recover the handwriting trajectory from the CIR time-series recorded while writing. The location of the writing object is estimated at each time instance and all such location estimates are accumulated to form a trajectory. This trajectory is further smoothed to obtain the final handwriting trajectory. An overview of the steps involved is shown in Fig. 3.

Let the CIR for each time instance t, recorded for all the 32 receiving antennas be denoted by $h[n_\mathrm{rx}, n, t]$, where n_rx is the receiving antenna index and n is the tap index of the CIR. The range could be estimated from the tap index. To extract the directional information, the received signals are spatially filtered by leveraging the phased array structure of the
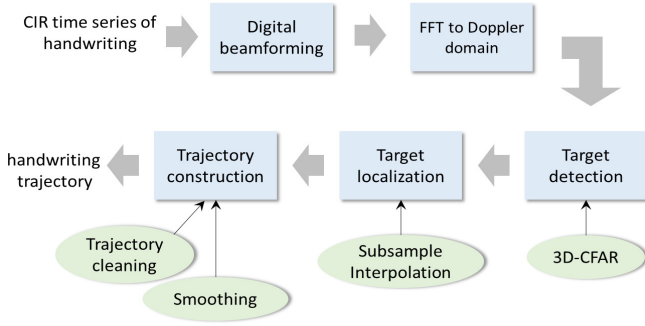
Fig. 3: Overview of handwriting tracking system.

antenna. This forms the first stage of the handwriting tracking algorithm.

A. Stage 1: Beamforming

Beamforming allows spatial filtering of signals arriving from different directions using a phased antenna array [13]. In this work, classical beamforming is used on the received CIR. Assuming K reflected signals which are incident on the receiving antenna array, the received signal h at the receiver n_{rx} can be modeled as:

$$h[n_{\mathrm{rx}}, n, t] = \sum_{k=1}^{K} a_{n_{\mathrm{rx}}}(az_k, el_k) g_k[az_k, el_k, n, t], \quad (1)$$

where g_k is the kth incoming reflected signal from azimuth and elevation angles az_k and el_k respectively, $a_{n_{\mathrm{rx}}}$ is the measured antenna response of the receiver n_{rx}, n is the CIR tap index and t is the time instance. The beamformed CIR $h_{\mathrm{bf}}[az, el, n, t]$ for the angle (az, el) is obtained by compensating for the array response as:

$$h_{\mathrm{bf}}[az, el, n, t] = \mathbf{a}^H(az, el)\mathbf{h}(., n, t), \quad (2)$$

where $\mathbf{a}(az, el)$ is the vector of antenna responses of all the receiver antennas for a signal arriving at an angle (az, el). To simplify the notation, a vector $\mathbf{T}$ is used to denote the triplet (az, el, n) as follows:

$$h[n_{\mathrm{rx}}, n, t] \overset{\text{beamforming}}{\longrightarrow} h_{\mathrm{bf}}[\underbrace{az, el, n}_{\mathbf{T}=[az, el, n]}, t] = h_{\mathrm{bf}}[\mathbf{T}, t]. \quad (3)$$

Utilizing the dynamic nature of the writing object, the proposed algorithm can differentiate the writing object from all the other static objects in the environment. This will be the aim of the second stage.

B. Stage 2: Transformation to Doppler domain

The correspondence between the relative velocity of the target and the observed frequency of the received signal, from the Doppler effect, motivated us to transform the beamformed signal to the frequency domain. This is achieved by performing a Fourier transform along the slow-time dimension t, using a moving window approach. The Fourier transform is applied in a window of length w_{l} and with a step size of w_{s}. A value of

$w_{\mathrm{l}} = 192$ and $w_{\mathrm{s}} = 32$ is used in this work. The transformation can be written as:

$$H_{\mathrm{bf}}[\mathbf{T}, f, s] \overset{FFT}{\longleftarrow} h_{\mathrm{bf}}[\mathbf{T}, t+(s-1)w_{\mathrm{s}}-w_{\mathrm{l}}+1 : t+(s-1)w_{\mathrm{s}}], \quad (4)$$

$$H_{\mathrm{bf}}[\mathbf{T}, f, s] \longleftrightarrow H_{\mathrm{bf}}[\mathbf{T}, v, s], \quad f = \frac{2v}{c}f_{\mathrm{o}}, \quad (5)$$

where H_{bf} is the transformed CIR, s is the window index, f_{o} is the carrier frequency, c is the speed of light, f is the Doppler frequency and v is the relative radial velocity of the target. Assuming a single moving target (e.g., the hand) in the field of view, the maximum power in the non-zero frequency bins is assumed to be corresponding to the target of interest. For each $\mathbf{T}$, the maximum power from different velocity bins is extracted as follows:

$$v_{\mathbf{T},s}^{\star} = \underset{v \neq 0}{\mathrm{argmax}}|H_{\mathrm{bf}}[\mathbf{T}, v, s]|, \quad (6)$$

$$\hat{H}_{\mathrm{bf}}[\mathbf{T}, s] = |H_{\mathrm{bf}}[\mathbf{T}, v_{\mathbf{T},s}^{\star}, s]|. \quad (7)$$

The extracted Doppler power is analyzed to detect the target in Stage 3.

C. Stage 3: Target detection

As the Doppler power spectrum is now available along with the range and spatial information, estimating the location of the peaks in the Doppler power spectrum can give the location of the target. However, the target may or may not be present at any given time instant and the maximum power could correspond to noise/interference. To avoid such false detections, the Doppler power is compared to a threshold. In real systems, the noise and interference are unknown and determining an absolute threshold is not relevant. This problem has been solved in the literature by using an adaptive threshold. The CA-CFAR (Cell Averaging-Constant False Alarm Rate) technique is one of the most widely used approaches in radar target detection systems [14].

A CFAR threshold map is computed for $\hat{H}_{\mathrm{bf}}[\mathbf{T}, s]$ and the maximum power exceeding the threshold is considered as corresponding to the target. Fig. 4a shows the Doppler power for different azimuth and elevation angles and a fixed range tap of 7 and the corresponding Doppler power with CFAR thresholding in Fig. 4b. The maximum power from the thresholded Doppler power is considered as corresponding to the target and the arguments indicate the location of the target. In this example, the target is located at an elevation of -8 degrees and an azimuth of -4 degrees with a Doppler power of 63.49 dB. The location of the target is indicated by the corresponding arguments as:

$$\mathbf{T}^{\star}(s) = \underset{\mathbf{T}}{\mathrm{argmax}}(\hat{H}_{\mathrm{bf}}[\mathbf{T}, s]), \quad (8)$$

where $\mathbf{T}^{\star}(s) = [az^{\star}(s), el^{\star}(s), r^{\star}(s)]$.
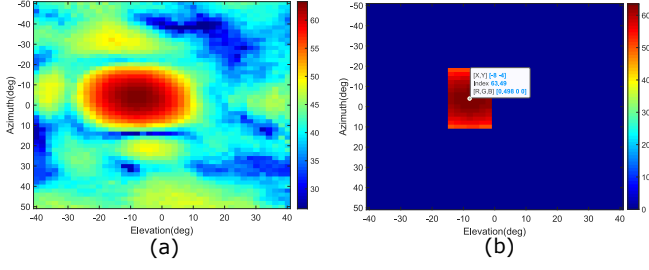
Fig. 4: (a) Doppler power at range tap 7 for different azimuth and elevation angles, (b) Doppler power after CFAR thresholding.

D. Stage 4: Target localization

At this point, the location estimate of the target can be obtained for each time instance. To further improve the accuracy of the location estimates, we leverage the observation that the Doppler power "flows" gradually from one bin to another since normal handwriting is generally smooth and continuous with no drastic movements.

The observation can be demonstrated by a simple experiment. Let us focus on the range dimension, for instance, and draw a straight line away from the device. Consider 3 taps at ranges 46.46 cm (tap 11), 51.12 cm (tap 12) and 55.38 cm (tap 13). As the target moves away from the device crossing the above ranges, a gradual change in the Doppler power is observed for the 3 taps as shown in Fig. 5a. Since we consider the tap with maximum Doppler power as that corresponding to the target, our range estimates are discrete as shown in the black solid line in Fig. 5a. Leveraging the observation that the Doppler power transition from one tap to another is smooth and continuous, the range estimate can further be improved using the Doppler power of the adjacent taps. Thus, a quadratic curve is fitted through the three values near the peak and the location of the vertex of the parabola is taken as the location of the peak. This technique is known as the sub-sample peak interpolation (SPI) as discussed in Section II. Fig. 5b shows the range estimates before and after SPI. In this work, SPI is applied to the range, azimuth and elevation dimension independently. Let $\mathbf{T}^{\star}_{a,b,c}(s) = [az^{\star}(s)+a, el^{\star}(s)+b, r^{\star}(s)+c]$ where a, b, c are the index offsets in the corresponding dimensions. The final estimates of azimuth, elevation and range coordinates are obtained from the SPI as:

$$az^{\star}_{\mathrm{I}}(s) = \mathrm{SPI}\{\hat{H}_{\mathrm{bf}}[\mathbf{T}^{\star}_{-1,0,0}(s), s],$$
$$\hat{H}_{\mathrm{bf}}[\mathbf{T}^{\star}_{0,0,0}(s), s], \qquad (9)$$
$$\hat{H}_{\mathrm{bf}}[\mathbf{T}^{\star}_{1,0,0}(s), s]\}$$

$$el^{\star}_{\mathrm{I}}(s) = \mathrm{SPI}\{\hat{H}_{\mathrm{bf}}[\mathbf{T}^{\star}_{0,-1,0}(s), s],$$
$$\hat{H}_{\mathrm{bf}}[\mathbf{T}^{\star}_{0,0,0}(s), s], \qquad (10)$$
$$\hat{H}_{\mathrm{bf}}[\mathbf{T}^{\star}_{0,1,0}(s), s]\}$$

$$r^{\star}_{\mathrm{I}}(s) = \mathrm{SPI}\{\hat{H}_{\mathrm{bf}}[\mathbf{T}^{\star}_{0,0,-1}(s), s],$$
$$\hat{H}_{\mathrm{bf}}[\mathbf{T}^{\star}_{0,0,0}(s), s], \qquad (11)$$
$$\hat{H}_{\mathrm{bf}}[\mathbf{T}^{\star}_{0,0,1}(s), s]\}.$$

At time instant s, the location $\mathbf{L}(s)$ of the moving target is given by $\mathbf{L}(s) = \mathbf{T}^{\star}_{\mathrm{I}}(s) = [az^{\star}_{\mathrm{I}}(s), el^{\star}_{\mathrm{I}}(s), r^{\star}_{\mathrm{I}}(s)]$ and the trajectory $\mathbf{P} = \{\mathbf{L}(s), \forall s \epsilon \mathbf{D}\}$, where $\mathbf{D}$ is the set of all time instances during handwriting.
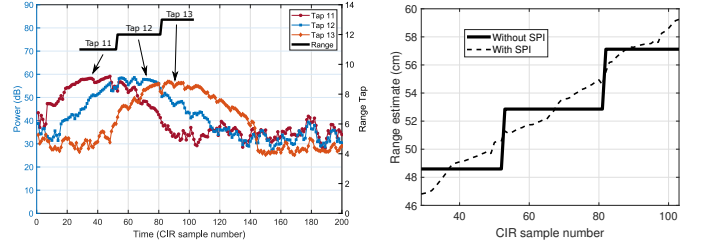

Fig. 5: (a) Doppler power for different range taps with time for a straight line drawn along the range away from the device, (b) Range estimates before and after SPI.

E. Stage 5: Trajectory construction

A raw trajectory can be constructed by combining the location estimates from Stage 4 at different instances of time. However, due to the difference in the point of reflection or missed target segments, outliers are possible. To minimize the effect of such outliers in the trajectory construction, trajectory cleaning is performed in two steps, (a) Power-based and (b) Range-based. These are demonstrated with an example. Consider a handwritten trajectory of the letter "h" whose range, azimuth and elevation estimates and the corresponding reflected power with time are shown in Fig. 6 and the corresponding projected 2D trajectory is shown in Fig. 7a. The outliers are marked as regions A and B. In the following steps, the procedure to remove the outliers is discussed.
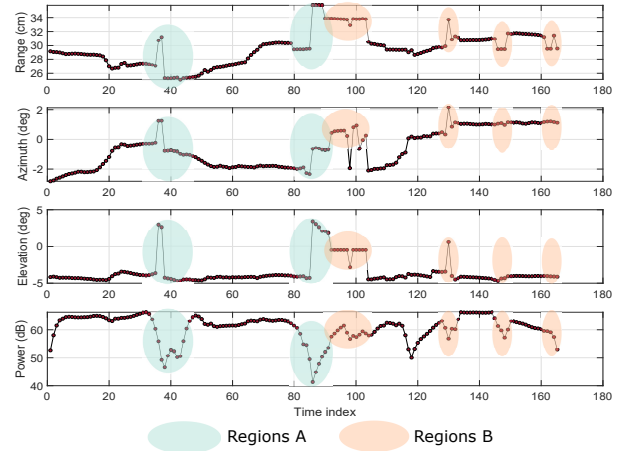

Fig. 6: Raw estimates of range, azimuth, elevation and power with outliers denoted by regions A and B.
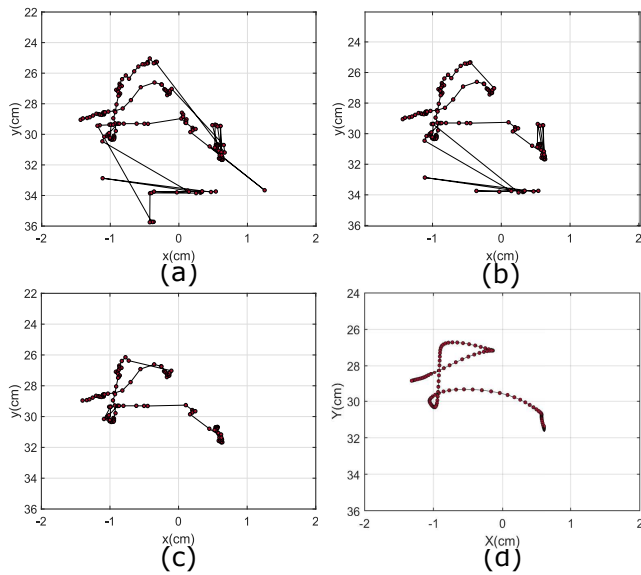
Fig. 7: Steps in trajectory construction. (a) Raw trajectory, (b) Trajectory after power-based cleaning, (c) Trajectory after power and range-based cleaning, (d) Trajectory after DCT-based smoothing.

- **Power-based**: In our algorithm, the segment of the pen/hand with maximum reflected power is tracked by the radar. In some instances, the reflected wave from that particular segment may not be received by the antenna and thus, the next highest reflected power is recorded. This results in outliers shown in region A, where a sudden decrease in the reflected power can be observed. Such points are removed by using the CFAR adaptive thresholding technique discussed in Stage 4. The resultant trajectory is shown in Fig. 7b.
- **Range-based**: For the outliers in region B, a sudden change in the range estimates can be observed. Such regions are filtered by using a tracking window. In this example, if the range estimate at the current time instant differs from the previous by greater than 1 cm, it is discarded. The resultant trajectory after range-based and power-based cleaning is as shown in Fig. 7c.

To further improve the smoothness of the recovered trajectory and robust removal of outliers, a smoothing technique is used on the recovered trajectory. Based on the cosine transformation, this technique computes the Discrete Cosine transform (DCT) of the data points, retains the higher and significant coefficients while discarding the non-significant coefficients which usually contain the noisy part of the signal [15]. The significant coefficients are then converted back to the data domain. Using a smoothing factor of 20, a smooth trajectory is obtained as shown in Fig. 7d.

IV. EXPERIMENTAL EVALUATION

To evaluate the performance of the proposed handwriting system, different experiments are conducted which will be discussed in this Section. The basic experimental setup is shown in Fig. 8 where the radar is placed on a table and the writing region is elevated so that the elevation angle is approximately zero. The writing is performed with natural speed using a marker on a paper. The smoothing parameter is automatically determined from the cross-validation score [15] unless mentioned otherwise.

Fig. 8: Experimental set up for handwriting tracking.

A. Performance

In this section, the performance of the proposed handwriting tracking system is evaluated using three different approaches.

1) **Visual inspection**: The trajectory traced by the proposed system is visually compared with the ground truth with respect to the shape of the trajectory. In the experiment, English alphabets are traced on a paper and the extracted trajectory is compared with the ground truth as shown in Fig. 9. It can be observed that the relative shape of the characters is preserved.

Fig. 9: Trajectories recovered from the proposed handwriting tracking system compared with the ground truth.

2) **Character recognition accuracy**: In this experiment, English alphabets are written in different sized grids and are traced multiple times. The obtained trajectory is fed to a standard handwriting recognition software (myScript). The character recognition accuracy from
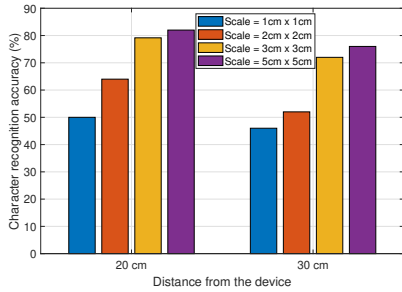
Fig. 10: Character recognition accuracy at different distances from the device with characters written in different scales.
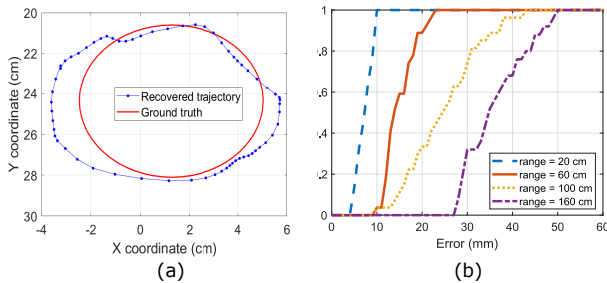

Fig. 11: (a) An example of a circle fit through the recovered trajectory points, (b) Cumulative distribution function of the tracking error at different ranges from the transceiver.

the software is reported and is shown in Fig. 10. The smoothing parameter s is set at 2. The figure shows recognition accuracy for 50 characters at different distances from the device and on different scales. The recognition accuracy decreases with distance and improves with increasing scale. For instance, the character recognition accuracy for characters written within 3 cm x 3 cm is 80% and 72% at distances 20 cm and 30 cm respectively. The recognition accuracy for the same distance of 20 cm is 80% and 82% for scales of 3 cm x 3 cm and 5 cm x 5 cm respectively. The recognition accuracy also depends on the classifier used in the recognition software and the values demonstrate the potential of the proposed handwriting tracking system in building smart surfaces.

3) **Tracking accuracy**: To estimate the tracking accuracy of the proposed system, a circle is traced several times on a paper and the corresponding trajectories are obtained. A circle with the measured radius is fit through the obtained trajectory points and the projected distance is reported as the tracking error. An example of the ground truth trajectory and the extracted trajectory is shown in Fig. 11a and the CDF of the errors are shown in Fig. 11b. The median error at distances of 30 cm, 70 cm, 120 cm, and 160 cm is 7.5 mm, 13.7 mm, 27.8 mm and 45.5 mm respectively which is about 2.5% of the distance from the radar. The 90 percentile error at distances of 30 cm, 70 cm, 120 cm, and 160 cm is 9.4

mm, 19.3 mm, 37.2 mm and 45.5 mm respectively.

V. CONCLUSIONS

In this work, we proposed a handwriting tracking system using a single commercial 60 GHz radar. Beamforming and radar target detection techniques allowed us to detect and track a moving/writing target. Further, post-processing of the obtained trajectory points using subsample peak interpolation and smoothing techniques could retrieve handwritten characters from regions as small as 1 cm x 1 cm. The performance of the proposed system is evaluated and discussed under different experimental conditions. With this, any flat surface can be a potential writing surface and the space for HCI can be extended much beyond the touch screens.

REFERENCES

[1] Jamie Shotton, Andrew W Fitzgibbon, Mat Cook, Toby Sharp, Mark Finocchio, Richard Moore, Alex Kipman, and Andrew Blake. Real-time human pose recognition in parts from single depth images. In *Cvpr*, volume 2, page 3, 2011.

[2] Jaime Lien, Nicholas Gillian, M Emre Karagozler, Patrick Amihood, Carsten Schwesig, Erik Olson, Hakim Raja, and Ivan Poupyrev. Soli: Ubiquitous gesture sensing with millimeter wave radar. *ACM Transactions on Graphics (TOG)*, 35(4):142, 2016.

[3] Nafiz Arica and Fatos T Yarman-Vural. An overview of character recognition focused on off-line handwriting. *IEEE Transactions on Systems, Man, and Cybernetics, Part C (Applications and Reviews)*, 31(2):216–233, 2001.

[4] Sandip Agrawal, Ionut Constandache, Shravan Gaonkar, Romit Roy Choudhury, Kevin Caves, and Frank DeRuyter. Using mobile phones to write in air. In *Proceedings of the 9th international conference on Mobile systems, applications, and services*, pages 15–28. ACM, 2011.

[5] Jue Wang, Deepak Vasisht, and Dina Katabi. Rf-idraw: virtual touch screen in the air using rf signals. In *ACM SIGCOMM Computer Communication Review*, volume 44, pages 235–246. ACM, 2014.

[6] Alexander Schick, Daniel Morlock, Christoph Amma, Tanja Schultz, and Rainer Stiefelhagen. Vision-based handwriting recognition for unrestricted text input in mid-air. In *Proceedings of the 14th ACM international conference on Multimodal interaction*, pages 217–220. ACM, 2012.

[7] Beibei Wang, Qinyi Xu, Chen Chen, Feng Zhang, and KJ Ray Liu. The promise of radio analytics: a future paradigm of wireless positioning, tracking, and sensing. *IEEE Signal Processing Magazine*, 35(3):59–80, 2018.

[8] KJ Ray Liu and Beibei Wang. *Wireless AI: Wireless Sensing, Positioning, IoT, and Communications*. Cambridge University Press, 2019.

[9] Teng Wei and Xinyu Zhang. mtrack: High-precision passive tracking using millimeter wave radios. In *Proceedings of the 21st Annual International Conference on Mobile Computing and Networking*, pages 117–129. ACM, 2015.

[10] L Svilainis and V Dumbrava. Analysis of the interpolation techniques for time-of-flight estimation. *Ultragarsas" Ultrasound"*, 63(4):25–29, 2008.

[11] Julius O Smith and Xavier Serra. Parshl: An analysis/synthesis program for non-harmonic sounds based on a sinusoidal representation. In *Proceedings of the 1987 International Computer Music Conference, ICMC; 1987 Aug 23-26; Champaign/Urbana, Illinois.[Michigan]: Michigan Publishing; 1987. p. 290-7*. International Computer Music Conference, 1987.

[12] Xiaoming Lai and Hans Torp. Interpolation methods for time-delay estimation using cross-correlation method for blood velocity measurement. *IEEE transactions on ultrasonics, ferroelectrics, and frequency control*, 46(2):277–290, 1999.

[13] Barry D Van Veen and Kevin M Buckley. Beamforming: A versatile approach to spatial filtering. *IEEE assp magazine*, 5(2):4–24, 1988.

[14] Mark A Richards. *Fundamentals of radar signal processing*. Tata McGraw-Hill Education, 2005.

[15] Damien Garcia. Robust smoothing of gridded data in one and higher dimensions with missing values. *Computational statistics & data analysis*, 54(4):1167–1178, 2010.